

Neutron Stars in Mimetic Gravity

Hajar Noshad^{1,2,3*}, Seyed Hossein Hendi^{1,2,4†} Behzad Eslam Panah^{4,5,6‡}

¹*Department of Physics, School of Science, Shiraz University, Shiraz 71454, Iran*

²*Biruni Observatory, School of Science, Shiraz University, Shiraz 71454, Iran*

³*Department of Physics, College of Science, Yasouj University, Yasouj, 75918-74934, Iran*

⁴*Canadian Quantum Research Center 204-3002 32 Ave Vernon, BC V1T 2L7 Canada*

⁴*Department of Theoretical Physics, Faculty of Science,*

University of Mazandaran, P.O. Box 47415-416, Babolsar, Iran

⁵*ICRANet-Babolsart, University of Mazandaran, P. O. Box 47415-416, Babolsar, Iran*

⁶*ICRANet, Piazza della Repubblica 10, I-65122 Pescara, Italy*

In this paper, a modified version of the hydrostatic equilibrium equation based on the mimetic gravity in the presence of perfect fluid is revisited. By using the different known equation of states, the structural properties of neutron stars are investigated in general relativity and mimetic gravity. Comparing the obtained results, we show that, unlike general relativity, we can find the appropriate equation of states that support observational data in the context of mimetic gravity. We also find that the results of relativistic mean-field-based models of the equation of states are in better agreement with observational data than non-relativistic models.

I. INTRODUCTION

General Relativity (GR) and its black hole solutions are interesting topics in gravitating systems. Despite having acceptable information from the region beyond the event horizon of black holes, the interior solution of horizonless massive objects is one of the open questions in physics. Indeed, the interior properties of stars and their time evolution are of interest during recent decades. The Tolman-Oppenheimer-Volkov (TOV) equation [1, 2] is one of the primitive attempts to describe the interior properties of spherical static perfect fluid objects. However, for solving the field equations and find the physical properties of a typical star, we have to consider an equation of state (EoS) explaining the relationship between two physical quantities; pressure and density.

We should emphasize that the interior solutions are based on three components: i) metric ansatz, ii) gravitational theory with an appropriate energy-momentum tensor such as GR with a perfect fluid which leads to the equation of hydrostatic equilibrium known as TOV, iii) EoS such as polytropic relation between pressure and density. Since the theoretical results of the TOV equation arisen from GR are not consistent with the observational evidence, different attempts have been considered to modified one (some) of the mentioned components. All these attempts are motivated by obtaining a better agreement between theory and observation, or testing alternative theories of gravitation. In this regard, different models of gravity are considered to investigate the compact objects and their modified TOV equations. For example neutron stars in an energy dependent spacetime are studied in Ref. [3]. Modified TOV equation in vector-tensor-Horndeski theory and dilaton gravity are reported in Refs. [4] and [5], respectively. Moreover, the neutron star structure is investigated in the context of $F(R)$, $F(G)$, $F(T)$, $F(R, T)$ and $F(R, L)$ theories of gravity [6–19]. Furthermore, neutron stars in massive gravity and magnetized neutron stars in gravity's rainbow are analyzed in [20] and [21], respectively. The structure of neutron stars in massive scalar-Gauss-Bonnet gravity is studied in Refs. [22–24]. Besides, neutron stars in the context of Eddington-inspired Born-Infeld theory of gravity are extracted in Refs. [25]. Considering the scalar-tensor theories of gravity, some interesting properties of neutron stars are studied in Refs. [26–31]. In addition, neutron star structure in Hořava and Hořava-Lifshitz theories of gravity are evaluated in Refs. [32] and [33], respectively. See Refs. [34–61] for additional information about neutron stars in modified gravity theories.

In this paper, we regard a modified TOV equation comes from the mimetic gravity in the presence of perfect fluid. As a matter of fact, mimetic gravity is a Weyl-symmetric extension of GR in which a dust-like perfect fluid can mimic cold dark matter from the cosmological point of view [62]. So, one of the main motivations of considering mimetic gravity is providing an interesting geometrical description for challenging topics such as the late-time acceleration [63], inflation [64] and dark matter [62]. Indeed, considering the mimetic scalar field in gravitating systems, one finds

* email address: noshad.hajar2@gmail.com

† email address: hendi@shirazu.ac.ir

‡ email address: eslampanah@umz.ac.ir

a dynamical longitudinal degree of freedom in addition to two traditional transverse degrees of freedom of GR. It is shown that such an additional degree of freedom could play the role of mimetic dark matter. The main idea of mimetic gravity backs to the interesting work of Chamseddine and Mukhanov [62], that proposed isolation of the conformal degree of freedom of gravity by introducing a parameterized physical metric $g_{\mu\nu}$ in terms of an auxiliary metric $\tilde{g}_{\mu\nu}$ and a (mimetic) scalar field ϕ , as follows

$$g_{\mu\nu} = -\tilde{g}_{\mu\nu} \tilde{g}^{\gamma\delta} \partial_\gamma \phi \partial_\delta \phi, \quad (1.1)$$

where confirms that the physical metric is invariant under conformal transformations of the auxiliary metric. Besides, taking a consistency condition into account, it is easy to show that the mimetic scalar field should satisfy the following constraint

$$g^{\gamma\delta} \partial_\gamma \phi \partial_\delta \phi = -1. \quad (1.2)$$

In this work, we follow the conventional notation of mimetic gravity in which this constraint can be appeared at the level of action formalism by including a Lagrange multiplier. Following Ref. [62], it is worth mentioning that the conformal degree of freedom becomes dynamical even in the absence of matter field, and therefore, the mimetic gravity may admit non-trivial solutions.

Motivated by what was mentioned above, the mimetic gravity has arisen a lot of attention in the past few years. From the cosmological point of view, it is a powerful theory to explain the flat rotation curves of spiral galaxies [65], gravitational wave [66, 67] and the cosmological singularity [68]. This theory can resolve the singularity in the center of black holes [69] and introduce new black hole solutions from the gravitational viewpoint. Thus, it will be interesting to investigate its effect on astrophysical objects such as neutron stars and study their structures.

Without exaggeration, neutron stars are proper laboratories to examine fundamental physics at high energy regime; from strong gravitational field to considerable nuclear densities. Actually, neutron stars help us to investigate the high density low temperature regime of matter field that is complementary to terrestrial laboratories. The density of neutron stars is distributed from few g/cm^3 to more than 10^{15}g/cm^3 at their surface and the center, respectively. The different layers of a neutron star can be categorized into the atmosphere, the outer and inner crusts, and also outer and inner cores. The outer crust can be described by comparing it with experimental data of atomic nuclei. Nevertheless, uncertainty in the EoS of neutron stars for regions with densities above nuclear matter density is still a substantial challenge since analyzing the astrophysical observations depends properly on the neutron star structure. So, there are different proposed EoSs that can describe the inner neutron stars with different structures such as the nucleon, hybrid, and the strange quark. The main theoretical techniques for determining EoSs are based on variational method, relativistic mean-field (RMF) models, effective interactions, perturbation expansion, effective energy-density functionals, and so on [70].

In this work, we consider the nuclear and hadronic stars which are in the range of the gravitational wave event GW170817 [71] and they have the maximum mass $M_{max} > 2M_\odot$. For pure nuclear matter, we consider different EoSs: SLy4 [72] of the Lyon group that is based on energy density functional, WFF1 [73] that is obtained by the variational method. We also include BSK21 [74] and MPA1 [75] constructed from the generalized Skyrme nuclear interaction arising from the Argonne V18 potential plus a microscopic nucleonic three-body force and Brueckner-Hartree-Fock theory, respectively. Besides, we choose the density-dependent relativistic mean-field (RMF) HS (DD2) EoS [76, 77] and the recently proposed FSU2H [78–80]. For the hadronic stars, we use various hadronic EoSs: $BH\Lambda\Phi$ [81] and SFHoY [76, 82, 83].

In this paper, we consider the different observational evidence of mass-radius relation of neutron stars, such as GW170817, PSR J0740 + 6620, PSR J2215 + 5135, NICER data on PSR J0030 + 0451 and GW190814. In fact, taking different observational data into account, we want to demonstrate how the mimetic gravity can be adapted to the appropriate EoS to obtain theoretical results consistent with observational evidence.

The outline of this paper is as follows. In the next section, we consider the spherically symmetric metric and obtain the required equations for solving, numerically, the generalized TOV in mimetic gravity. In section III, we introduce a set of nuclear matter EoSs and three potentials to drive $M - R$ diagrams and discuss the properties of neutron stars. Finally, we finish our paper with conclusions.

II. HYDROSTATIC EQUILIBRIUM EQUATION IN MIMETIC GRAVITY

The starting point is the action of mimetic gravity in four dimension in the presence of a matter field as

$$S = \frac{c^4}{16\pi G} \int d^4x \sqrt{-g} [\mathcal{R} + \lambda (g^{\mu\nu} \partial_\mu \phi \partial_\nu \phi - \epsilon) - V(\phi)] + \mathcal{I}_m, \quad (2.1)$$

where \mathcal{R} and ϕ are, respectively, the Ricci scalar and the mimetic scalar field, λ is the Lagrange multiplier while the constant $\epsilon = \pm 1$ can be fixed by spacelike or timelike nature of $\partial_\mu \phi$. Besides, $V(\phi)$ is the potential related to the mimetic scalar field and \mathcal{I}_m denotes the action of matter field which we consider it as a perfect fluid. It is straightforward to vary the action (2.1) with respect to the metric tensor $g_{\mu\nu}$ and the mimetic scalar field ϕ to obtain the equations of motion as

$$G_{\mu\nu} = \lambda \partial_\mu \phi \partial_\nu \phi - \frac{1}{2} V(\phi) g_{\mu\nu} + \kappa T_{\mu\nu}, \quad (2.2)$$

$$\frac{1}{\sqrt{-g}} \partial^\mu (\sqrt{-g} \lambda \partial_\mu \phi) = -\frac{1}{2} \frac{dV(\phi)}{d\phi}, \quad (2.3)$$

where $\kappa = \frac{8\pi G}{c^4}$ and G is the four dimensional gravitational constant. In addition, $G_{\mu\nu}$ is the Einstein tensor and $T_{\mu\nu} = \frac{-2}{\sqrt{-g}} \frac{\delta \mathcal{I}_m}{\delta g^{\mu\nu}}$ is the energy-momentum tensor with the following explicit form

$$T^{\mu\nu} = \left(\rho + \frac{P}{c^2}\right) u^\mu u^\nu - P g^{\mu\nu}, \quad (2.4)$$

where ρ and P are, respectively, the density and pressure of the perfect fluid measuring by a local observer, and u^ν is the fluid four-velocity ($u_\nu u^\nu = c^2$). Moreover, one can vary the above action with respect to the Lagrange multiplier to obtain

$$g_{\mu\nu} \partial^\mu \phi \partial^\nu \phi = \epsilon. \quad (2.5)$$

Taking the trace of Eq. (2.2) and inserting Eq. (2.5), one finds

$$\lambda = \frac{(G_\alpha^\alpha - \kappa T_\alpha^\alpha + 2V)}{\epsilon}. \quad (2.6)$$

Now, we can insert λ (Eq. (2.6)) into the field equations to achieve

$$G_{\mu\nu} - \epsilon (G_\alpha^\alpha - \kappa T_\alpha^\alpha + 2V) \partial_\mu \phi \partial_\nu \phi + \frac{1}{2} g_{\mu\nu} V(\phi) - \kappa T_{\mu\nu} = 0, \quad (2.7)$$

$$\frac{\epsilon}{\sqrt{-g}} \partial^\mu (\sqrt{-g} [G_\alpha^\alpha - \kappa T_\alpha^\alpha + 2V] \partial_\mu \phi) + \frac{1}{2} \frac{dV(\phi)}{d\phi} = 0. \quad (2.8)$$

In order to find the equation of hydrostatic equilibrium for compact stars, we have to regard a suitable line element. Here, we assume a spherical symmetric spacetime with the following ansatz

$$ds^2 = c^2 f(r) dt^2 - \frac{dr^2}{g(r)} - r^2 (d\theta^2 + \sin^2 \theta d\varphi^2), \quad (2.9)$$

where we should analyze the properties of the radial metric functions $f(r)$ and $g(r)$. Using the metric introduced in Eq. (2.9), we can obtain the components of energy-momentum tensor (2.4) as

$$T_0^0 = c^2 \rho \quad \& \quad T_1^1 = T_2^2 = T_3^3 = -P. \quad (2.10)$$

Taking into account Eq. (2.5) with the metric ansatz (2.9), the mimetic scalar field can be given by the spatial metric function with the following form

$$\phi(r) = \int \left(\frac{-\epsilon}{g(r)} \right)^{\frac{1}{2}} dr. \quad (2.11)$$

Inserting the metric ansatz (2.9) with Eqs. (2.10) and (2.11) into the gravitating field equation, we can simplify the components of Eq. (2.7)

$$eq_1 = -\kappa c^2 \rho r^2 + \frac{1}{2} V(\phi) r^2 - r g' - g + 1 = 0, \quad (2.12)$$

$$eq_2 = \left[r^2 g^2 (2f f'' - f'^2) + r^2 g f f' \left(g' + \frac{4g}{r} \right) + 2f^2 g \left(\kappa r^2 \left\{ c^2 \rho - 3P - \frac{2V}{\kappa} \right\} + [2r(g-1)]' \right) \right] \phi'^2 + 2\epsilon r f g f' + \epsilon f^2 (-2\kappa r^2 P - r^2 V + 2g - 2) = 0, \quad (2.13)$$

$$eq_3 = r f g f'' - \frac{r g}{2} f'^2 + \frac{f f'}{2} (r g' + 2g) - f^2 (2\kappa r P + r V - g') = 0, \quad (2.14)$$

where f , g , ρ and P are functions of r and also the prime and double prime are, respectively, the first and second derivatives with respect to r . Taking Eq. (2.11) into account, we can remove ϕ' in Eq. (2.13) as follows

$$eq_2 = 2r^2 f g f'' - r^2 g f'^2 + r f f' (r g' + 2g) + f^2 (2\kappa c^2 r^2 \rho - 4\kappa r^2 P - 3r^2 V + 4r g' + 2g - 2). \quad (2.15)$$

Considering Eq. (2.12) as a differential equation, we can obtain $g(r)$ as a function of from ρ and $V(\phi)$

$$g(r) = 1 - \frac{1}{r} \kappa c^2 \int \rho r^2 dr + \frac{1}{2r} \int r^2 V(\phi) dr. \quad (2.16)$$

Now, we derive, algebraically, $g'(r)$ from Eq. (2.12) and regard $g(r)$ from Eq. (2.16), and insert them into Eq. (2.15). After some manipulations, we can find that Eq. (2.15) can be rewritten as

$$\begin{aligned} eq_2 = & \left(\frac{r^2 f'^2 - r f f''}{2} - r^2 f f'' + f^2 \right) \int r^2 V(\phi) dr + r^3 (f'^2 - 2f f'') \left(1 - \frac{\kappa M c^2}{4\pi r} \right) + \\ & r f f' \left(c^2 \kappa r^3 \rho + \frac{\kappa M c^2}{4\pi} - \frac{1}{2} r^3 V(\phi) - 2r \right) + r^3 f^2 \left(V(\phi) + 2\kappa \left[\rho c^2 + 2P - \frac{M c^2}{4\pi r^3} \right] \right) = 0, \end{aligned} \quad (2.17)$$

where $M = \int 4\pi r^2 \rho dr$. Here, we can define a new variable $w = \frac{df}{dr}$ to change Eq. (2.17) into the following first-order differential equation

$$\begin{aligned} eq_2 = & \left(\frac{r^2 w^2 - r f w}{2} - r^2 f w' + f^2 \right) \int r^2 V(\phi) dr + r^3 (w^2 - 2f w') \left(1 - \frac{\kappa M c^2}{4\pi r} \right) + \\ & r f w \left(c^2 \kappa r^3 \rho + \frac{\kappa M c^2}{4\pi} - \frac{1}{2} r^3 V(\phi) - 2r \right) + r^3 f^2 \left(V(\phi) + 2\kappa \left[\rho c^2 + 2P - \frac{M c^2}{4\pi r^3} \right] \right) = 0. \end{aligned} \quad (2.18)$$

Now, we are in a position to talk about the equation of hydrostatic equilibrium by use of the conservation of energy-momentum tensor, $\nabla_\mu T^{\mu\nu} = 0$, in which for $\nu = r$, we can write

$$\frac{dP}{dr} = -(P + \rho c^2) \frac{f'}{2f}. \quad (2.19)$$

Now, we have Eqs. (2.11), (2.12), (2.18), (2.19) and we should solve them numerically for a given EoS ($P(\rho)$).

III. EOS, NEUTRON STAR STRUCTURE AND OBSERVATIONAL DATA

There is a theoretical challenge to applying a proper EoS for the description of the internal structure of neutron stars. Here, we consider different known models of EoS in the context of GR and mimetic gravity to obtain an appropriate conclusion. So far, a large number of the EoS with various motivations have been introduced, and in this paper, we examine eight relativistic/non-relativistic EoSs that seem more realistic and have already received more attention.

The first non-relativistic EoS is SLy4 has been derived from energy density functional methods with an effective nucleon-nucleon interaction [72]. The second model of non-relativistic EoSs refers to BSK21 that is constructed from the generalized Skyrme nuclear interaction arising from the Argonne V18 potential plus a microscopic nucleonic three-body force [74]. The third non-relativistic model is defined according to a variational method known as WFF1 [73].

Now, we point out the relativistic category of EoSs that we considered in this paper. The first model is devoted to MPA1 arising from the relativistic Dirac-Brueckner-Hartree-Fock approach with the π - ρ mesons exchange [75]. We also choose the HS (DD2) EoS [76, 77] as the second model of this category that is based on the density-dependent relativistic mean-field (RMF) interactions of Typel et al. [84]. The third model is known as FSU2H EoS. The nucleonic FSU2 model of [85] is modified in the context of relativistic mean-field theory to describe both the nucleon and hyperon interactions, and so FSU2H EoS is created [78–80].

We also use two hadronic EoSs, $BH\Lambda\Phi$ [81] and SFHoY [76, 82, 83], as other realistic models. The $BH\Lambda\Phi$ EoS additionally includes Λ hyperons and hyperon-hyperon interactions mediated by Φ mesons. The Λ hyperon makes the EoS stiffer resulting in $2.1M_\odot$ maximum mass neutron star corresponding to a radius 11.58 km . Also, SFHoY is based on the statistical model with an excluded volume and interactions of Hempel and Schaffner-Bielich (HS) [76] with RMF interactions SFHo [83]. Although these EoSs are obtained with RMF interactions, we may exclude them from the full relativistic category since they are formulated in densities below saturation density and low temperatures.

TABLE I: The maximum mass and corresponding radius for the different EoSs in GR.

GR	$M_{max} (M_{\odot})$	$R (km)$
SLy4	2.05	10.00
WFF1	2.12	9.48
BSK21	2.28	11.02
MPA1	2.49	11.35
DD2	2.42	11.90
$BHB\Lambda\Phi$	2.10	11.58
FSU2H	2.37	12.43
SFHoY	1.99	10.52

Before proceeding, it is notable that we examine the mentioned models of EoSs with different accepted functions of scalar potentials $V(\phi)$.

It is worth mentioning that in this paper, for nucleonic EoSs, we use from the parameterized piecewise-polytrope representation applied in [86–88], which we now describe in brief.

A piecewise polytropic EoS with four segment pieces satisfy the following polytropic relation,

$$P(\rho) = \begin{cases} K_0 \rho^{\Gamma_0} & \rho \leq \rho_0 \\ K_1 \rho^{\Gamma_1} & \rho_0 \leq \rho \leq \rho_1 \\ K_2 \rho^{\Gamma_2} & \rho_1 \leq \rho \leq \rho_2 \\ K_3 \rho^{\Gamma_3} & \rho > \rho_2 \end{cases} \quad (3.1)$$

where P is the fluid pressure, and K_i and Γ_i denote, respectively, the polytropic constant and the adiabatic index. The first polytrope piece shows the crust EoS that is determined by $K_0 = 35939 \times 10^{13} [\text{cgs}]$ and $\Gamma_0 = 13572$ [86]. Furthermore, two dividing high densities between core pieces are chosen as $\rho_1 = 10^{14.7} g/cm^3$ and $\rho_2 = 10^{15} g/cm^3$. In this method, for a chosen of four free parameters $P_1, \Gamma_1, \Gamma_2, \Gamma_3$ (where $P_1 = P(\rho_1)$ and Γ_1, Γ_2 and Γ_3 are the adiabatic indices) and by considering the continuity of the pressure, we can fix the polytropic constants K_1, K_2 , and K_3 in the following form

$$P(\rho_i) = K_i \rho^{\Gamma_i} = K_{i+1} \rho^{\Gamma_{i+1}}. \quad (3.2)$$

Considering the mentioned points and following Ref. [86], the parameterized EoS is completely determined (For the details see Ref. [86]).

Moreover, taking the GR limit into account, one can find that all of the chosen EoSs are in the range of the gravitational wave event GW170817 [71] and they produce a neutron star with maximum mass $M_{max} > 2m_{\odot}$. However, these EoSs did not support some of the observational evidence (see Fig. 1 and table I for more details).

Before comparing the results of neutron star properties in GR and mimetic gravity, we should note that in Figs. 1-5, we consider 1σ (63%) and 2σ (95%) mass-radius constraints from the gravitational wave event GW170817 by the blue and orange clouded regions corresponding to the heavier and lighter neutron stars, respectively [71]. In these figures, the purple region also shows the 1σ and 2σ confidential levels of the massive pulsar PSR J0740+6620 with mass $2.14^{+0.20}_{-0.18} M_{\odot}$ [89]. Also, we illustrate the mass range of the pulsar PSR J2215+5135 [90], with a mass $2.27 M_{\odot}$, by light green region in the mentioned figures. Besides, regarding these figures, the black error bars and the red band show the NICER (Neutron Star Interior Composition Explorer) mass-radius measurement on PSR J0030+0451 [91, 92] and GW190814 event [93], respectively.

Since we have the results of different EoSs in GR, here, we use the modified theory of gravity (mimetic gravity) to calculate the mass-radius relation for each EoS to find matching with the observational data. Strictly speaking, we investigate the mass-radius relation of neutron stars in mimetic gravity for three scalar potentials; $V_1(\phi) = \frac{\alpha_1}{\phi^2}$, $V_2(\phi) = \frac{\alpha_2}{e^{K\phi^2}}$, and $V_3(\phi) = \frac{\alpha_3 \phi^2}{1 + e^{K\phi^2}}$. Therefore, we have the free parameters $\alpha_i (i = 1, 2, 3)$ and $\phi(0)$ that can affect more or less the maximum mass and radius of the neutron stars (Note: $\phi(0) = \phi(r)|_{r=0}$ is the initial value of mimetic scalar field at the center of the neutron star which should be fixed for numerical analysis).

The first step is devoted to considering one of the well-known EoSs, SLy4 EoS. It is easy to show that in the GR limit, this EoS can reach $2M_{\odot}$ and it is within the GW170817 region. However, the mass-radius relation of this EoS could not support one of the ranges of J0030+0451 error bars. For SLy4 EoS, we plot the $M - R$ relation for potentials $V_1(\phi)$, $V_2(\phi)$ and $V_3(\phi)$ in Fig. 2 with $\phi(0) = 1$ (left panels) and $\phi(0) = 0.8$ (right panels). We observe for $\phi(0) = 1$, the maximum mass generally increases by increasing the parameter α_i . Recall that the sign of α_i is negative, and hereafter, we discuss the absolute value of α_i for the sake of simplicity. The increase of the mass at $V_3(\phi)$ is greater than $V_1(\phi)$ and $V_2(\phi)$. In order to have a easier comparison, we calculate the maximum mass and radius for three

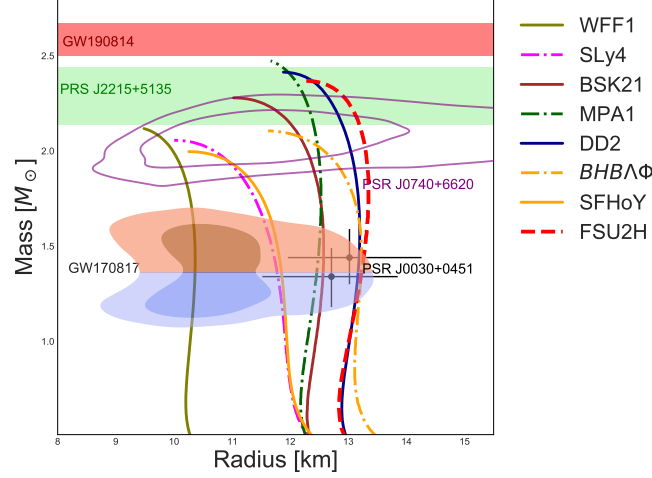


FIG. 1: The mass-radius diagram of neutron stars in GR for the different EoSs. The blue and orange regions are the mass-radius constraints from the GW170817 event. The purple region represents the pulsar J0740+6620 and the light green region amounts to the pulsar J2215+5135 and also the black dots with error bars, are the NICER estimations of PSR J0030+0451. The mass of the compact object observed by the GW190414 event is shown as a red band.

TABLE II: M_{max} and corresponding radius for *non-relativistic EoSs* with $K = 0.5$, $\phi(0) = 1$ ($\phi(0) = 0.8$) and various $\alpha_i (i = 1..3)$.

SLy4	$V_1(\phi) = \frac{\alpha_1}{\phi^2}$		$V_2(\phi) = \frac{\alpha_2}{e^{K\phi^2}}$		$V_3(\phi) = \frac{\alpha_3\phi^2}{1+e^{K\phi^2}}$	
$\phi(0) = 1$ (0.8)	$M_{max} (M_\odot)$	$R (km)$	$M_{max} (M_\odot)$	$R (km)$	$M_{max} (M_\odot)$	$R (km)$
$\alpha_i = -0.01$	2.06(2.06)	10.02(10.02)	2.05(2.06)	9.99(10.00)	2.06(2.06)	10.00(10.02)
$\alpha_i = -0.05$	2.07(2.07)	10.17(10.21)	2.06(2.07)	10.01(10.04)	2.08(2.09)	10.08(10.12)
$\alpha_i = -0.10$	2.08(2.09)	10.40(10.49)	2.07(2.08)	10.03(10.10)	2.11(2.14)	10.18(10.23)
BSK21	$V_1(\phi) = \frac{\alpha_1}{\phi^2}$		$V_2(\phi) = \frac{\alpha_2}{e^{K\phi^2}}$		$V_3(\phi) = \frac{\alpha_3\phi^2}{1+e^{K\phi^2}}$	
$\phi(0) = 1$ (0.8)	$M_{max} (M_\odot)$	$R (km)$	$M_{max} (M_\odot)$	$R (km)$	$M_{max} (M_\odot)$	$R (km)$
$\alpha_i = -0.01$	2.28(2.28)	11.10(11.10)	2.28(2.28)	11.02(11.06)	2.28(2.28)	11.06(11.07)
$\alpha_i = -0.05$	2.30(2.30)	11.28(11.34)	2.29(2.29)	11.05(11.09)	2.31(2.32)	11.14(11.15)
$\alpha_i = -0.10$	2.32(2.34)	11.56(11.64)	2.30(2.31)	11.08(11.12)	2.33(2.36)	11.22(11.28)
WFF1	$V_1(\phi) = \frac{\alpha_1}{\phi^2}$		$V_2(\phi) = \frac{\alpha_2}{e^{K\phi^2}}$		$V_3(\phi) = \frac{\alpha_3\phi^2}{1+e^{K\phi^2}}$	
$\phi(0) = 1$ (0.8)	$M_{max} (M_\odot)$	$R (km)$	$M_{max} (M_\odot)$	$R (km)$	$M_{max} (M_\odot)$	$R (km)$
$\alpha_i = -0.01$	2.13(2.15)	9.32(9.33)	2.13(2.13)	9.30(9.30)	2.13(2.13)	9.30(9.30)
$\alpha_i = -0.05$	2.15(2.17)	9.61(9.64)	2.15(2.15)	9.36(9.36)	2.16(2.18)	9.37(9.45)
$\alpha_i = -0.10$	2.18(2.21)	9.95(10.08)	2.16(2.18)	9.36(9.43)	2.20(2.22)	9.51(9.60)

different values for α_i and two values for $\phi(0)$ in table II. Considering the reported maximum mass, one can find that the larger one belongs to potential $V_3(\phi)$. Furthermore, according to Fig. 2, we can find that by increasing of $|\alpha_i|$, there is a small increment in the radius corresponding to potential $V_2(\phi)$ and a bigger one corresponding to $V_1(\phi)$ and $V_3(\phi)$. Therefore, considering the potentials $V_1(\phi)$ and $V_3(\phi)$ for $\alpha_i = -0.05, -0.10$ ($i = 1, 3$), not only the curves are still within the GW170817 region, but also it can reach both the PSR J0030 + 0451 error bars.

We also consider the case $\phi(0) = 0.8$ in right panels of Fig. 2. Obviously, the mass-radius yields a similar behavior as in the previous case $\phi(0) = 1$, i.e., as we increase the value of parameter α_i , an enhancement is observed in the maximum mass. However, by comparing the left and right panels of Fig. 2, one finds that reducing $\phi(0)$ leads to increasing the maximum mass. Such a result can be confirmed by comparison of maximum masses for $\phi(0) = 1$ and $\phi(0) = 0.8$ in table II more clearly. It is observed that for potential $V_3(\phi)$ ($|\alpha_3| = 0.1$), the maximum mass reaches $2.14M_\odot$, so in addition to the fact that it still lies within two GW170817 and NICER regions, it also reaches the PSR J2215 + 5135.

In order to investigate the effect of MPA1 EoS on the neutron star structure, we plot the corresponding mass-radius relation in Fig. 3. By increasing parameter α_i or reducing $\phi(0)$, the mass-radius relation yields a similar behavior such as previous case (the SLy4 case). Also, similar to the SLy4 case, we observe a greater maximum mass for potential

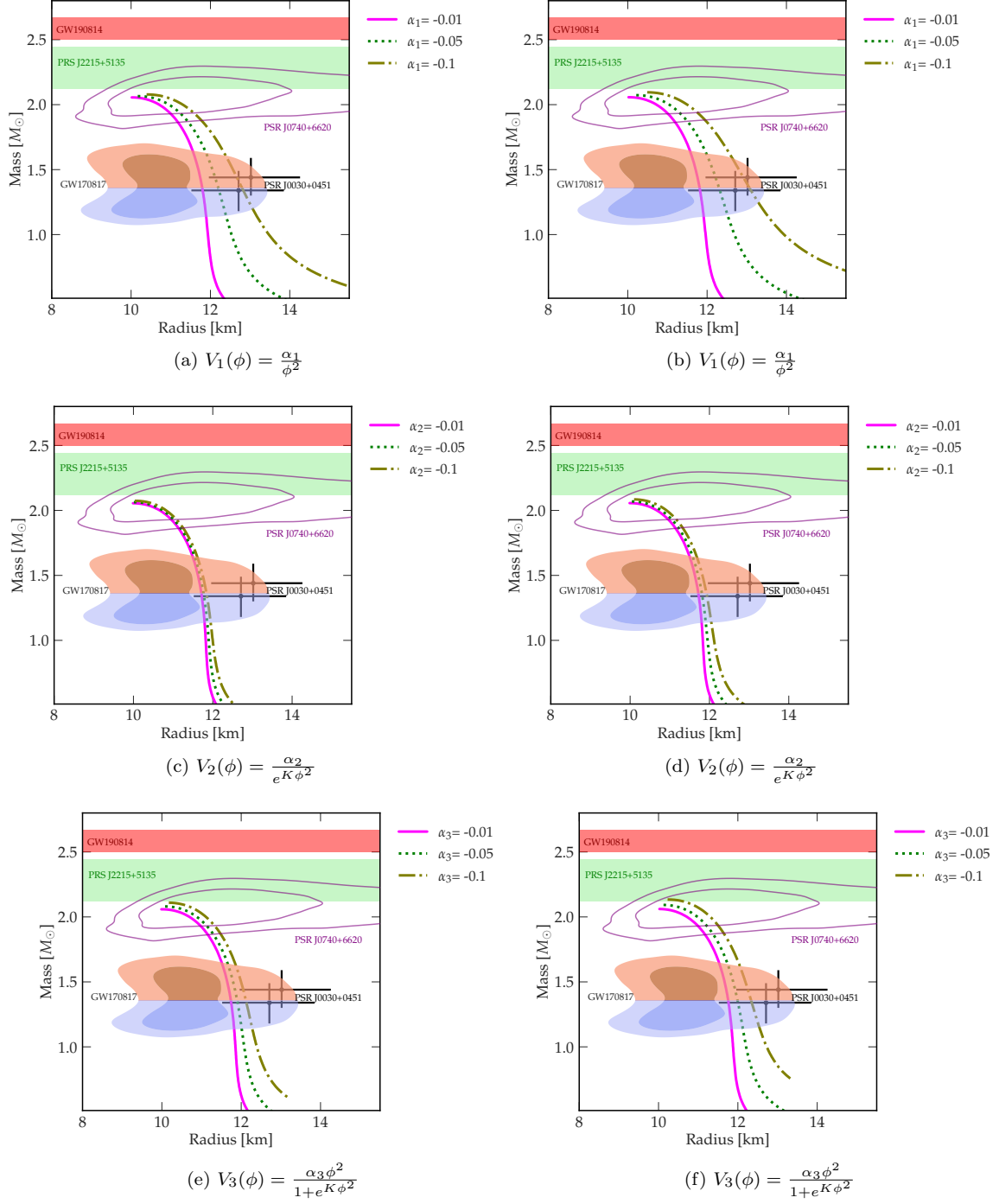


FIG. 2: The mass-radius relation of neutron stars in mimetic gravity for SLy4 EoS. $\phi(0) = 1$: left panels and $\phi(0) = 0.8$: right panels and $K = 0.5$.

$V_3(\phi)$ comparing to the potentials $V_2(\phi)$ and $V_1(\phi)$ (see table III for more details). It is notable that the curves for all three potentials can support all the observation regions. However, some of the curves for parts (a) and (b) of Fig. 3 is discredited, since it lies out of the LIGO-VIRGO region. As a final result, it is worth mentioning that to support all observational evidence within this EoS, the best value of parameter α_1 is about -0.05 for potential $V_1(\phi)$.

Following the previous calculations, we investigate the mass-radius behaviour of neutron stars for the BSK21 EoS in Fig. 4 and table III. It is worth mentioning that similar to the case of MPA1 EoS, there are some curves for parts (a) and (b) of Fig. 4 that are out of LIGO-VIRGO data, and therefore, parameter α_i can be considered around -0.05

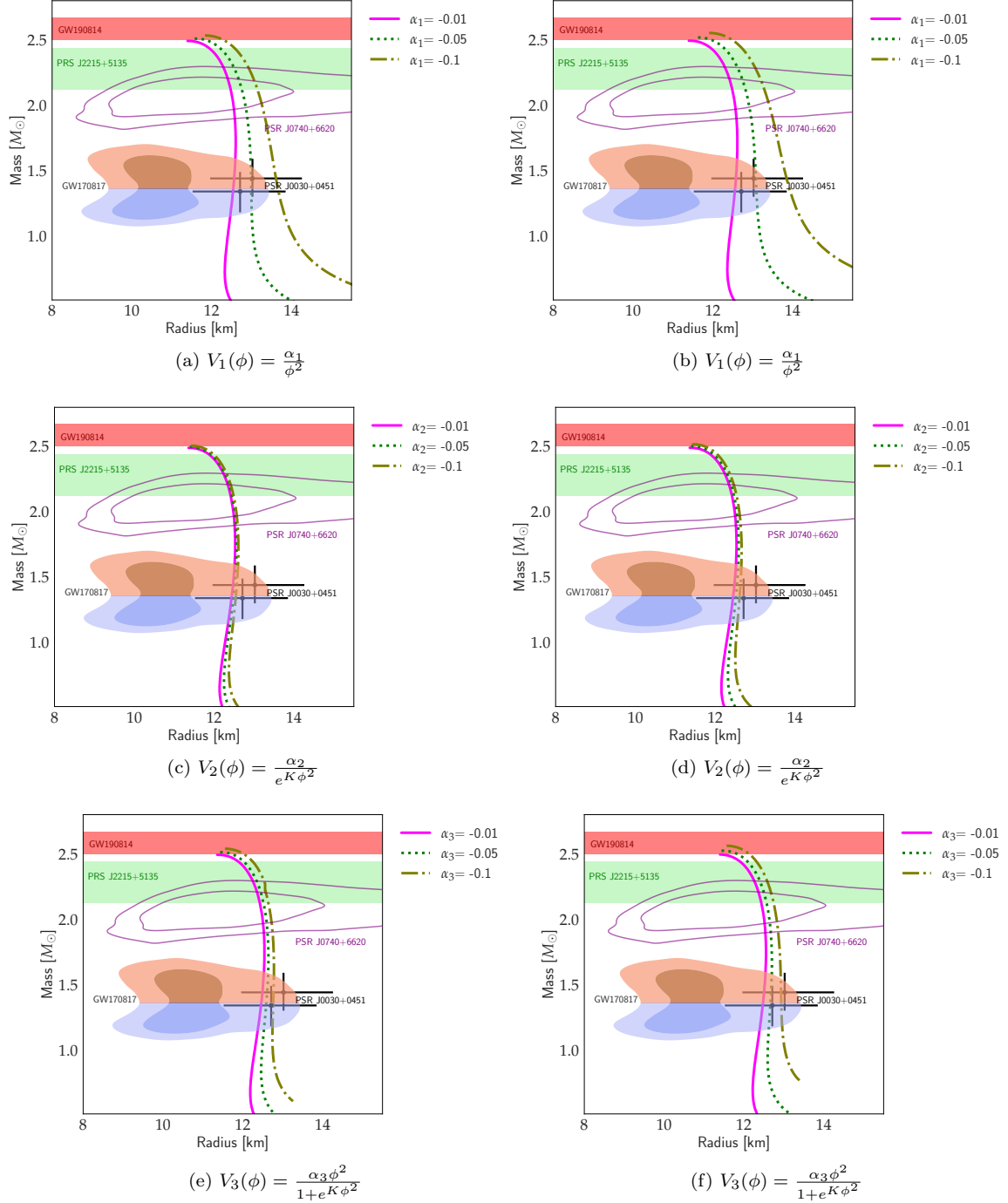


FIG. 3: The mass-radius relation of neutron stars in mimetic gravity for MPA1 EoS. $\phi(0) = 1$: left panels and $\phi(0) = 0.8$: right panels and $K = 0.5$.

which is similar to MPA1 EoS.

We desire to investigate the mass-radius relation for WFF1 EoS that is reflected in Fig. 5. The general behavior of the mass-radius relation is similar to those of the previous EoSs, i.e., increasing $|\alpha_i|$ leads to increasing maximum mass (see table II). It is also observed that for GR limit this EoS could not support the pulsar J2215+5135 and its radius is small (see Fig. 1). So it could not reach NICER observations. Taking Fig. 5 into account, we find that in mimetic gravity for all three potentials, for large α_i , the maximum mass is within the pulsar J2215+5135 region. Besides, for potential $V_1(\phi)$ and by considering $\phi(0) = 1$, the mass-radius plot supports the first NICER error bar,

TABLE III: M_{max} and corresponding radius for *relativistic EoSs* with $K = 0.5$, $\phi(0) = 1$ ($\phi(0) = 0.8$) and various $\alpha_i (i = 1..3)$

MPA1	$V_1(\phi) = \frac{\alpha_1}{\phi^2}$		$V_2(\phi) = \frac{\alpha_2}{e^{K\phi^2}}$		$V_3(\phi) = \frac{\alpha_3\phi^2}{1+e^{K\phi^2}}$	
$\phi(0) = 1$ (0.8)	$M_{max} (M_\odot)$	$R (km)$	$M_{max} (M_\odot)$	$R (km)$	$M_{max} (M_\odot)$	$R (km)$
$\alpha_i = -0.01$	2.50(2.49)	11.39(11.40)	2.49(2.49)	11.36(11.36)	2.49(2.50)	11.36(11.40)
$\alpha_i = -0.05$	2.51(2.52)	11.57(11.63)	2.50(2.50)	11.39(11.39)	2.51(2.52)	11.43(11.44)
$\alpha_i = -0.10$	2.53(2.55)	11.83(11.90)	2.51(2.52)	11.42(11.42)	2.54(2.56)	11.51(11.56)
DD2	$V_1(\phi) = \frac{\alpha_1}{\phi^2}$		$V_2(\phi) = \frac{\alpha_2}{e^{K\phi^2}}$		$V_3(\phi) = \frac{\alpha_3\phi^2}{1+e^{K\phi^2}}$	
$\phi(0) = 1$ (0.8)	$M_{max} (M_\odot)$	$R (km)$	$M_{max} (M_\odot)$	$R (km)$	$M_{max} (M_\odot)$	$R (km)$
$\alpha_i = -0.01$	2.42(2.43)	11.93(11.93)	2.42(2.42)	11.89(11.89)	2.43(2.44)	11.89(11.89)
$\alpha_i = -0.05$	2.44(2.46)	12.18(12.20)	2.43(2.44)	11.88(11.87)	2.45(2.47)	11.97(11.97)
$\alpha_i = -0.10$	2.47(2.51)	12.38(12.52)	2.44(2.45)	11.95(11.95)	2.48(2.52)	11.94(12.05)
FSU2H	$V_1(\phi) = \frac{\alpha_1}{\phi^2}$		$V_2(\phi) = \frac{\alpha_2}{e^{K\phi^2}}$		$V_3(\phi) = \frac{\alpha_3\phi^2}{1+e^{K\phi^2}}$	
$\phi(0) = 1$ (0.8)	$M_{max} (M_\odot)$	$R (km)$	$M_{max} (M_\odot)$	$R (km)$	$M_{max} (M_\odot)$	$R (km)$
$\alpha_i = -0.01$	2.40(2.40)	12.57(12.58)	2.39(2.39)	12.53(12.52)	2.40(2.41)	12.56(12.56)
$\alpha_i = -0.05$	2.42(2.43)	12.81(12.87)	2.40(2.40)	12.51(12.55)	2.42(2.43)	12.59(12.59)
$\alpha_i = -0.10$	2.45(2.49)	13.15(13.30)	2.41(2.43)	12.59(12.57)	2.48(2.51)	12.66(12.71)

TABLE IV: M_{max} and corresponding radius for *hadronic EoSs* with $K = 0.5$, $\phi(0) = 1$ ($\phi(0) = 0.8$) and various $\alpha_i (i = 1..3)$.

$BHB\Lambda\Phi$	$V_1(\phi) = \frac{\alpha_1}{\phi^2}$		$V_2(\phi) = \frac{\alpha_2}{e^{K\phi^2}}$		$V_3(\phi) = \frac{\alpha_3\phi^2}{1+e^{K\phi^2}}$	
$\phi(0) = 1$ (0.8)	$M_{max} (M_\odot)$	$R (km)$	$M_{max} (M_\odot)$	$R (km)$	$M_{max} (M_\odot)$	$R (km)$
$\alpha_i = -0.01$	2.11(2.12)	11.52(11.58)	2.11(2.11)	11.47(11.47)	2.11(2.12)	11.47(11.47)
$\alpha_i = -0.05$	2.13(2.15)	11.86(11.93)	2.12(2.13)	11.50(11.55)	2.14(2.16)	11.61(11.61)
$\alpha_i = -0.10$	2.17(2.21)	12.34(12.05)	2.14(2.16)	11.58(11.62)	2.18(2.22)	11.68(11.81)
SFHoY	$V_1(\phi) = \frac{\alpha_1}{\phi^2}$		$V_2(\phi) = \frac{\alpha_2}{e^{K\phi^2}}$		$V_3(\phi) = \frac{\alpha_3\phi^2}{1+e^{K\phi^2}}$	
$\phi(0) = 1$ (0.8)	$M_{max} (M_\odot)$	$R (km)$	$M_{max} (M_\odot)$	$R (km)$	$M_{max} (M_\odot)$	$R (km)$
$\alpha_i = -0.01$	2.00(2.00)	10.27(10.27)	2.00(2.00)	10.23(10.23)	2.00(2.00)	10.23(10.23)
$\alpha_i = -0.05$	2.02(2.03)	10.48(10.53)	2.01(2.02)	10.26(10.29)	2.03(2.04)	10.29(10.34)
$\alpha_i = -0.10$	2.04(2.06)	10.78(10.90)	2.03(2.04)	10.32(10.34)	2.06(2.08)	10.40(10.49)

while by changing $\phi(0)$ to 0.8, we find that both of NICER error bars are supported by mass-radius diagram.

Also, we investigate the DD2 EoS in Fig. 6 in mimetic gravity. It is seen that this EoS can reach the GW190814 event for all potentials. However, for $V_1(\phi)$ model with $\alpha_1 = -0.1$, we observe that radii are large and the mass-radius diagram cannot support the GW170817 region. As for the final nucleonic EoS, we consider the FSU2H EoS in Fig. 7. It can be seen that for $V_3(\phi)$, by increasing α , the maximum mass lies in the GW190814 observations while it could not reach this region in GR limit. Furthermore, for all of potentials, the radii of this hadronic EoS increase and they are not in the GW170817 region anymore.

In Fig. 8 and 9, the mass-radius curves are exhibited for hadronic EoSs $BHB\Lambda\Phi$ and SFHoY. We calculate maximum mass and radius for different values of α and potentials in table IV. According to Fig. 1, in the GR limit, the maximum mass of star for $BHB\Lambda\Phi$ could not reach the PSR J2215+5135. However, according to Fig. 8 we observe that the maximum mass is reached in this region for all of $V_1(\phi)$, $V_2(\phi)$ and $V_3(\phi)$ potentials. But the radius for $V_1(\phi)$ is expanded and it is out of GW170817 event. Nevertheless, for the $V_2(\phi)$ and $V_3(\phi)$ potentials, the curves still lie in the GW170817 region.

The second hadronic EoS is SFHoY EoS. In Fig 9, it can be observed this EoS supports the first or even second NICER error bars in mimetic gravity by increasing $|\alpha|$. But in GR limit, it does not lie in this region. In addition, for all of choice of α parameter and all potentials $V_1(\phi)$, $V_2(\phi)$ and $V_3(\phi)$, the curves support the GW170817 event.

In order to compare the effectiveness of different EoSs, we collect the results of GR and mimetic gravity in table V. In general, we find that mimetic gravity can improve the results and it can support more observational evidence than GR case. Besides, it is evident that MPA1, DD2 and FSU2H EoSs in the context of mimetic gravity can support the mentioned observational data as indicated in table V. According to this interesting result, we focus on these three EoSs to drive other physical properties of neutron stars such as Schwarzschild radius, redshift and compactness.

Schwarzschild radius: considering the obtained function $g(r)$ in Eq. (2.16), and using the horizon radius constraint ($g(r)|_{r=R} = 0$), we can extract the Schwarzschild radius (R_{Sch}). It is clear that by applying the mimetic

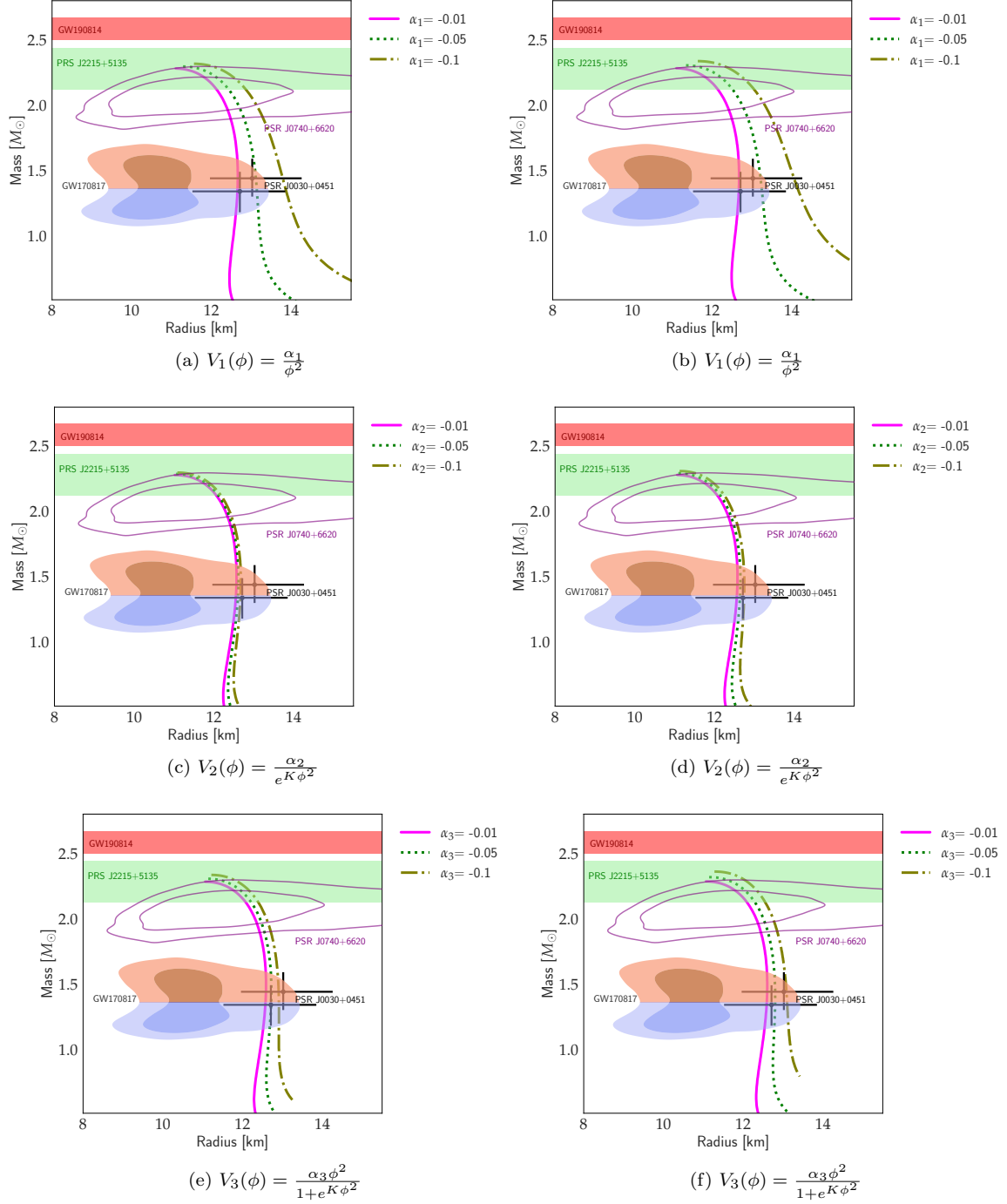


FIG. 4: The mass-radius relation of neutron stars in mimetic gravity for BSK21 EoS. $\phi(0) = 1$: left panels and $\phi(0) = 0.8$: right panels and $K = 0.5$.

scalar field (Eq. (2.11)), and using $g(r)|_{r=R} = 0$, the mentioned scalar potentials become zero on surface of neutron star, i.e., $V(\phi)|_{r=R} = 0$. Therefore, we obtain the Schwarzschild radius for the mimetic gravity (which is the same GR gravity) as

$$R_{Sch} = \frac{2GM}{c^2}. \quad (3.3)$$

As one can see in the equation (3.3) and tables VI-VIII, by increasing maximum mass of neutron star, the Schwarzschild radius increases.

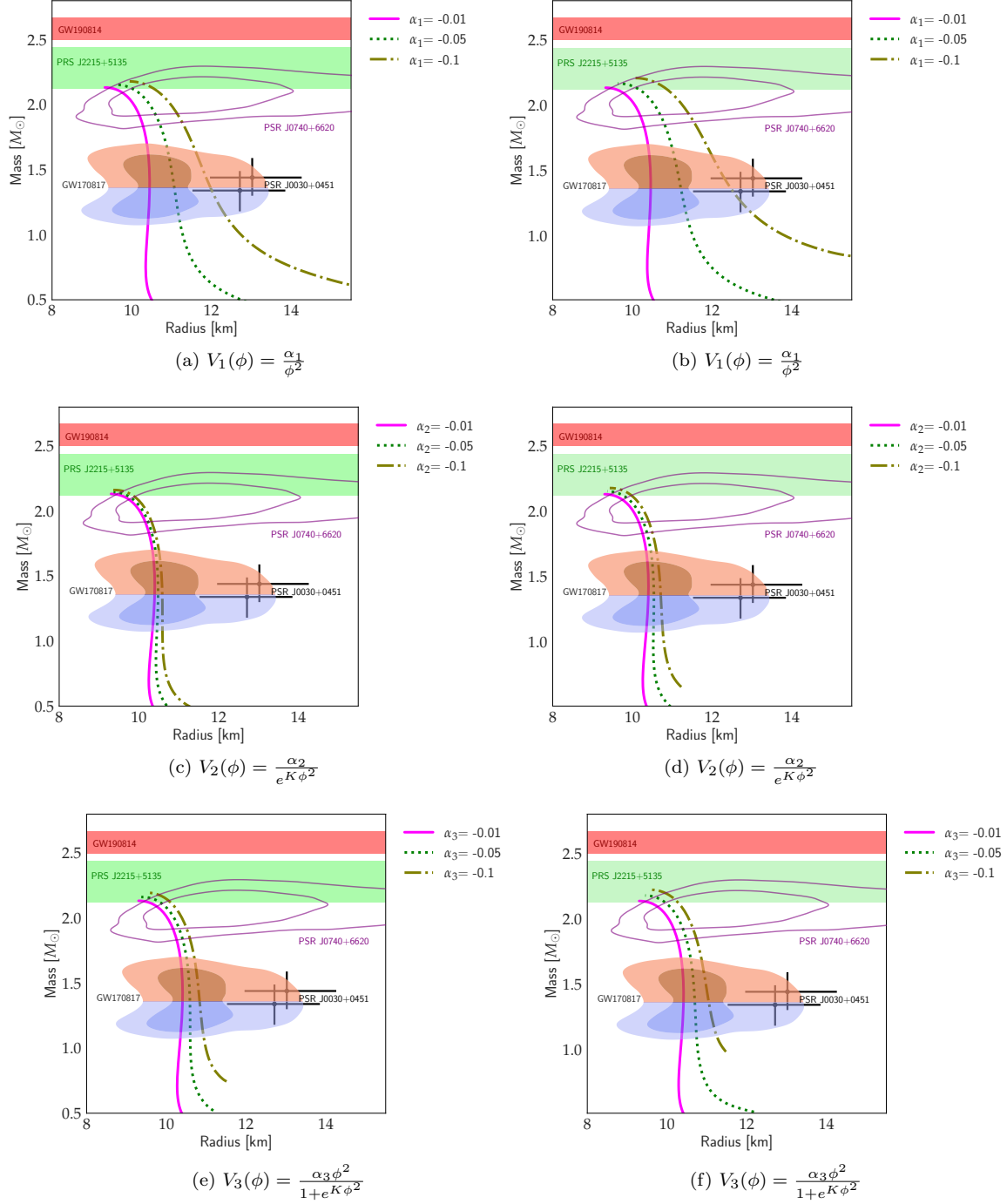


FIG. 5: The mass-radius relation of neutron stars in mimetic gravity for WFF1 EoS. $\phi(0) = 1$: left panels and $\phi(0) = 0.8$: right panels and $K = 0.5$.

Gravitational redshift and compactness: other important quantities in which we intend to extract them, are related to the gravitational redshift and compactness of neutron stars in the mimetic gravity. These quantities may give us information about the strength of gravity of neutron star.

We use from definition of the gravitational redshift and this fact that the mentioned scalar potentials are zero on

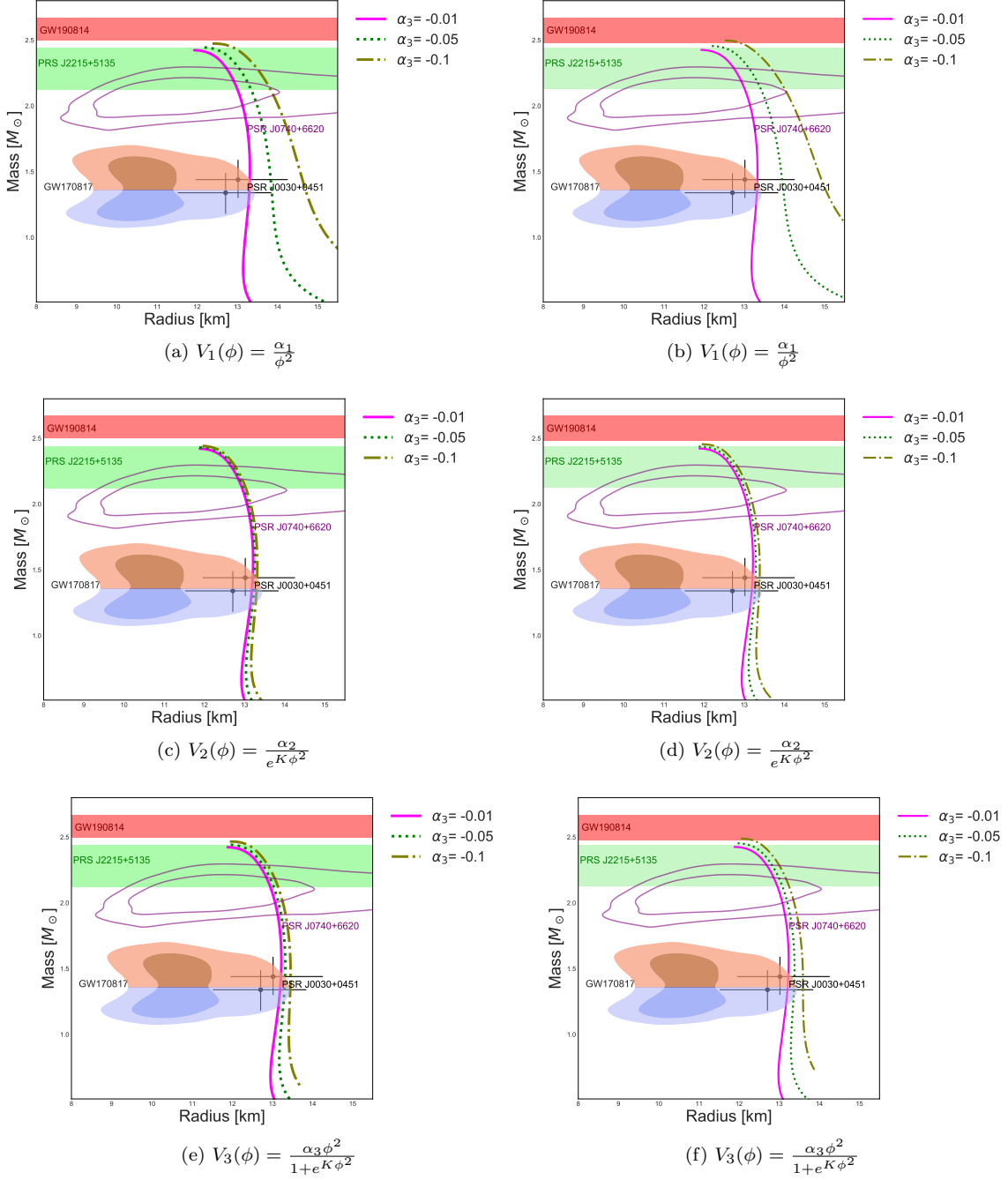


FIG. 6: The mass-radius relation of neutron stars in mimetic gravity for DD2 EoS. $\phi(0) = 1$: left panels and $\phi(0) = 0.8$: right panels and $K = 0.5$.

surface of neutron star, we extract the gravitational redshift as

$$z = \frac{1}{\sqrt{1 - \frac{2GM}{c^2 R}}} - 1, \quad (3.4)$$

where R is radius of neutron star.

The compactness of a spherical compact object may be defined by the ratio of the mass to radius of that compact

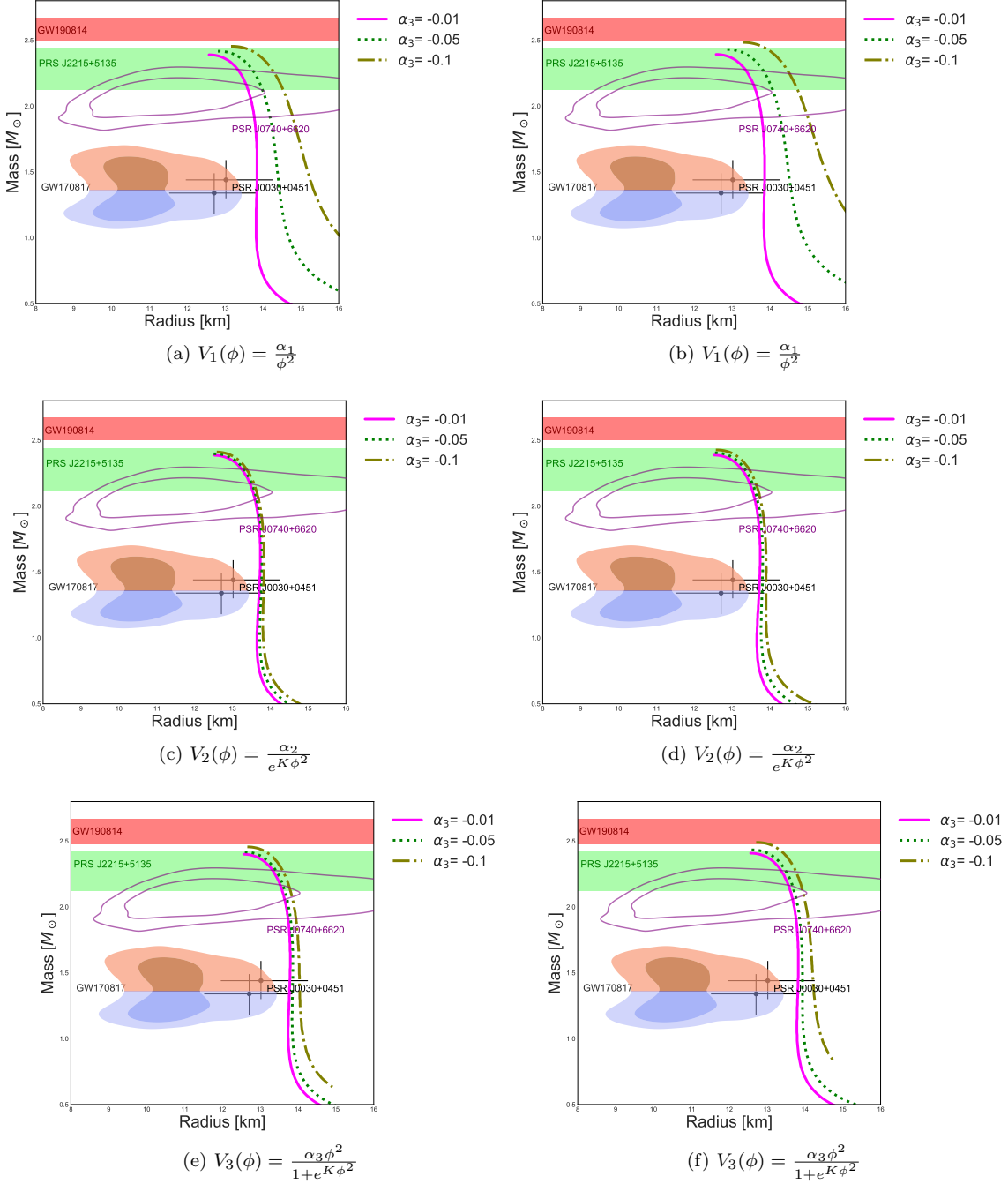


FIG. 7: The mass-radius relation of neutron stars in mimetic gravity for FSU2H EoS. $\phi(0) = 1$: left panels and $\phi(0) = 0.8$: right panels and $K = 0.5$.

object

$$\sigma = \frac{GM}{c^2 R}. \quad (3.5)$$

Now, we are in a position to investigate the gravitational redshift and compactness of the obtained neutron stars of MPA1 EoS in the mimetic gravity. Considering Eqs. (3.4), (3.5), and the obtained results in table III, we find an interesting property of neutron stars. The gravitational redshift and compactness of neutron star in the mimetic gravity are dependent on the scalar potential models. In other words, there are two different manners for these quantities. They decrease by increasing the maximum mass of neutron star in $V_1(\phi)$ model. However, they increase

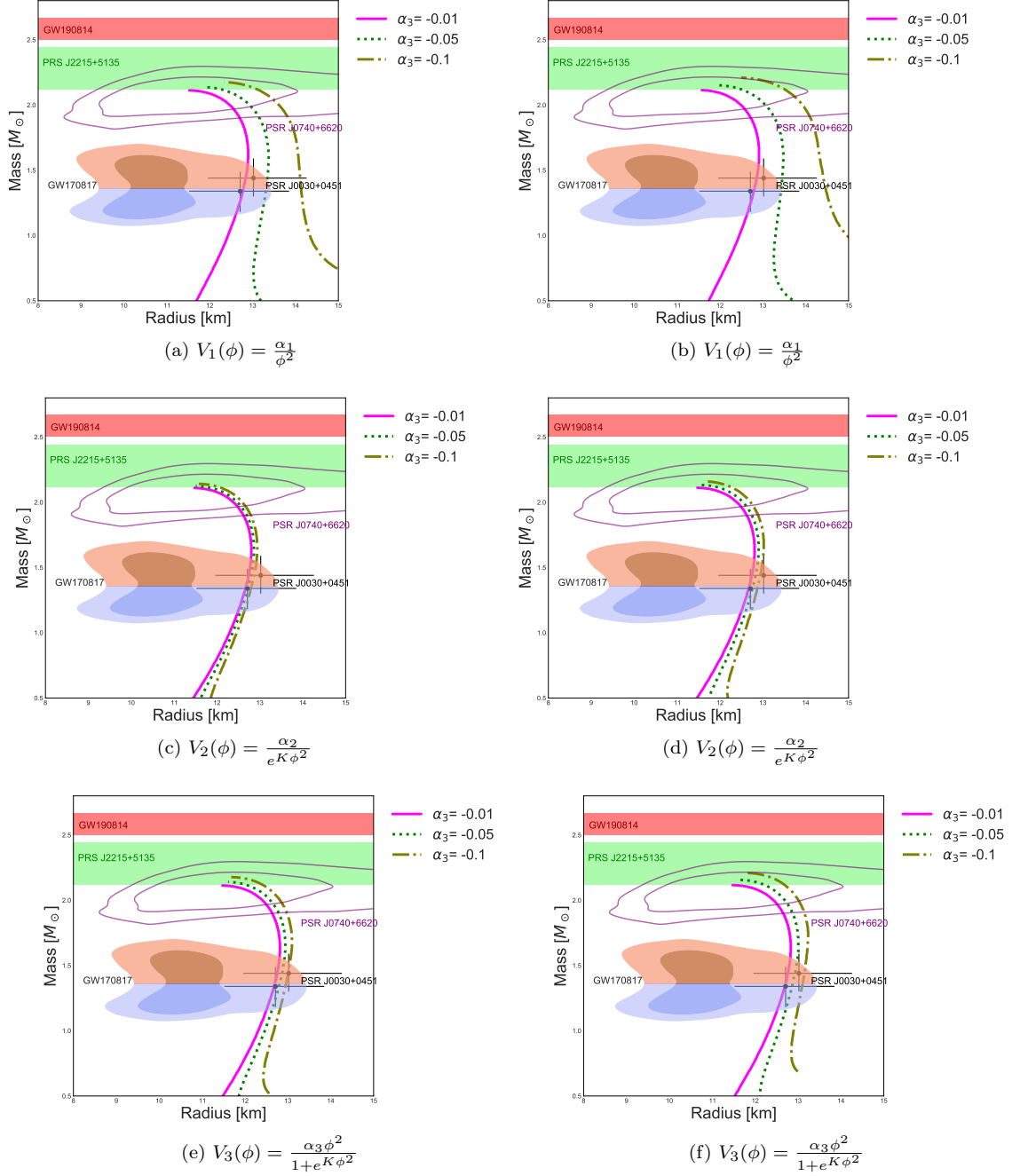


FIG. 8: The mass-radius relation of neutron stars in mimetic gravity for $BHB\Lambda\phi$ EoS. $\phi(0) = 1$: left panels and $\phi(0) = 0.8$: right panels and $K = 0.5$.

by increasing the maximum mass for $V_2(\phi)$ and $V_3(\phi)$ models (see table VI, for more details). In addition, there are the same behavior for DD2 and FSU2H EoSs (see tables VII-VIII, for more details). Therefore the gravitational redshift and compactness of neutron stars in the mimetic gravity are completely depending on the scalar potential models.

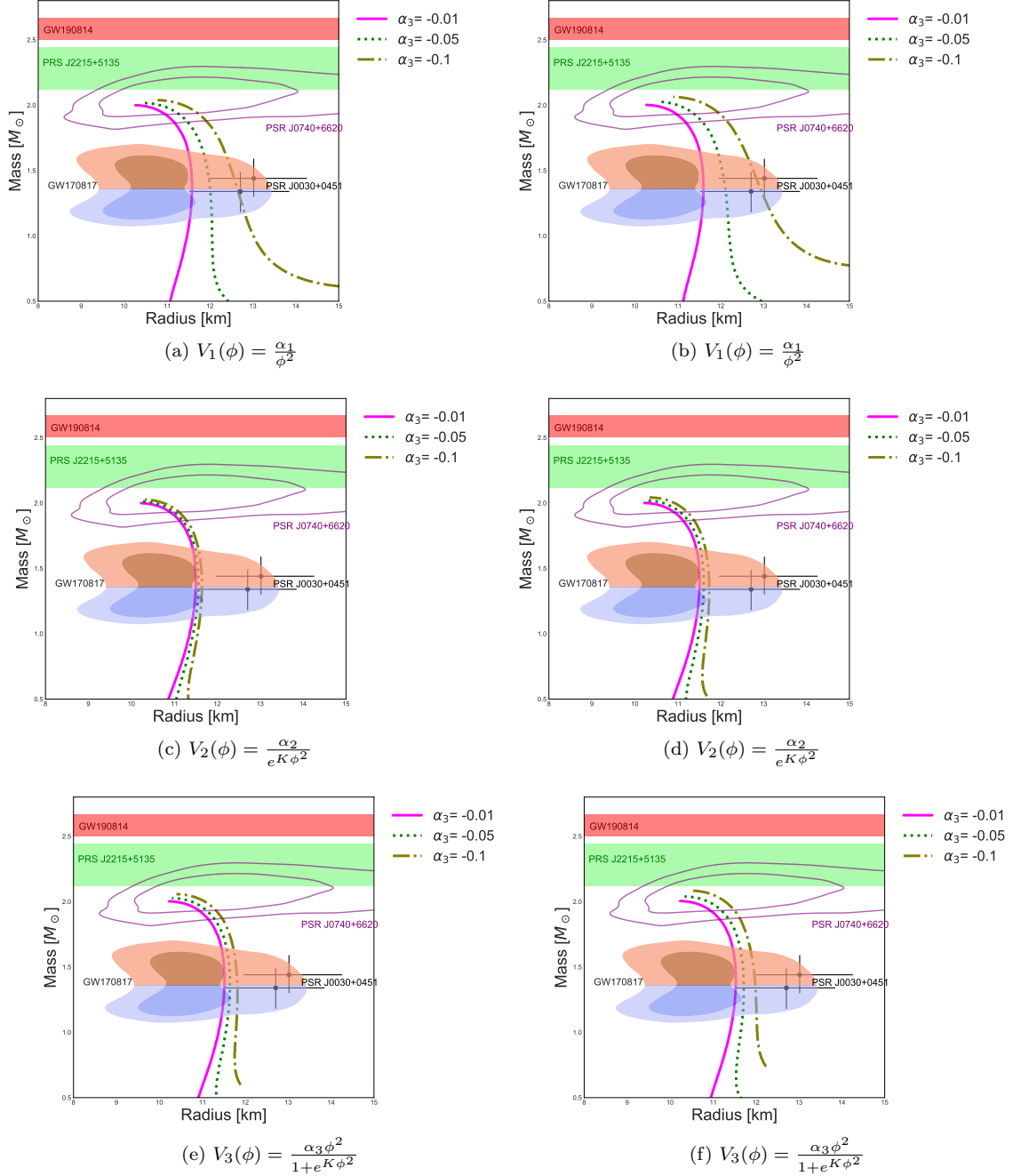


FIG. 9: The mass-radius relation of neutron stars in mimetic gravity for SFHoY EoS. $\phi(0) = 1$: left panels and $\phi(0) = 0.8$: right panels and $K = 0.5$.

IV. CONCLUSION

The study of neutron stars, one of the possible endpoints of stellar evolution, is an interesting hot topic in physics communities since they provide a natural laboratory for the investigation of high density and pressure medium. The neutron star structure can be considered from theoretical and observational perspectives. In recent years, different properties of diverse neutron stars are accessible from the observational evidence, such as GW170817, PSR J0740+6620, PSR J2215+5135, NICER data on PSR J0030+0451 and GW190814. However, from theoretical point of view, different EoSs in the context of GR and other modified theories of gravitation could not support all observational data, simultaneously. Therefore, to describe the neutron stars, research on suitable EoS and appropriate theory

TABLE V: The different observation data for the different EoSs in GR and mimetic gravity.

GR	GW170817	GW190814	PSR J0740+6620	PSR J2215+5135	PSR J0030+04511 (the first error bar)	PSR J0030+04511 (the second error bar)
SLy4	✓	×	✓	×	✓	×
MPA1	✓	×	✓	✓	✓	✓
BSK21	✓	×	✓	✓	✓	✓
WFF1	✓	×	✓	×	×	×
DD2	✓	×	✓	✓	✓	✓
$BHB\Lambda\Phi$	✓	×	✓	×	✓	✓
FSU2H	✓	×	✓	✓	✓	✓
SFHoY	✓	×	✓	×	✓	×
Mimetic gravity	GW170817	GW190814	PSR J0740+6620	PSR J2215+5135	PSR J0030+0451 (the first error bar)	PSR J0030+0451 (the second error bar)
SLy4	✓	×	✓	✓	✓	✓
MPA1	✓	✓	✓	✓	✓	✓
BSK21	✓	×	✓	✓	✓	✓
WFF1	✓	×	✓	✓	✓	✓
DD2	✓	✓	✓	✓	✓	✓
$BHB\Lambda\Phi$	✓	×	✓	×	✓	✓
FSU2H	✓	✓	✓	✓	✓	✓
SFHoY	✓	×	✓	×	✓	✓

TABLE VI: Structure properties of neutron star in mimetic gravity for MPA1 EoS with $\phi(0) = 1$ ($\phi(0) = 0.8$) and $K = 0.5$.

$V_1(\phi) = \frac{\alpha_1}{\phi^2}$	$M_{max} (M_\odot)$	$R (km)$	$R_{Sch} (km)$	$\sigma(10^{-1})$	$z(10^{-1})$
$\alpha_1 = -0.01$	2.50(2.49)	11.39(11.40)	7.37(7.34)	3.24(3.22)	6.83(6.76)
$\alpha_1 = -0.05$	2.51(2.52)	11.57(11.63)	7.40(7.43)	3.20(3.19)	6.66(6.64)
$\alpha_1 = -0.10$	2.53(2.55)	11.83(11.90)	7.46(7.52)	3.16(3.16)	6.45(6.48)
$V_2(\phi) = \frac{\alpha_2}{e^{K\phi^2}}$	$M_{max} (M_\odot)$	$R (km)$	$R_{Sch} (km)$	$\sigma(10^{-1})$	$z(10^{-1})$
$\alpha_2 = -0.01$	2.49(2.49)	11.36(11.36)	7.34(7.34)	3.23(3.23)	6.81(6.81)
$\alpha_2 = -0.05$	2.50(2.50)	11.39(11.39)	7.37(7.37)	3.24(3.24)	6.83(6.83)
$\alpha_2 = -0.10$	2.51(2.52)	11.42(11.42)	7.40(7.43)	3.24(3.25)	6.85(6.92)
$V_3(\phi) = \frac{\alpha_3\phi^2}{1+e^{K\phi^2}}$	$M_{max} (M_\odot)$	$R (km)$	$R_{Sch} (km)$	$\sigma(10^{-1})$	$z(10^{-1})$
$\alpha_3 = -0.01$	2.49(2.50)	11.36(11.40)	7.34(7.37)	3.23(3.23)	6.81(6.82)
$\alpha_3 = -0.05$	2.51(2.52)	11.43(11.44)	7.40(7.43)	3.24(3.25)	6.84(6.89)
$\alpha_3 = -0.10$	2.54(2.56)	11.51(11.56)	7.49(7.55)	3.26(3.26)	6.92(6.98)

TABLE VII: Structure properties of neutron star in mimetic gravity for DD2 EoS with $\phi(0) = 1$ ($\phi(0) = 0.8$) and $K = 0.5$.

$V_1(\phi) = \frac{\alpha_1}{\phi^2}$	$M_{max} (M_\odot)$	$R (km)$	$R_{Sch} (km)$	$\sigma(10^{-1})$	$z(10^{-1})$
$\alpha_1 = -0.01$	2.42(2.43)	11.93(11.93)	7.13(7.16)	2.99(3.00)	5.78(5.82)
$\alpha_1 = -0.05$	2.44(2.46)	12.18(12.20)	7.19(7.25)	2.95(2.97)	5.63(5.70)
$\alpha_1 = -0.10$	2.47(2.51)	12.38(12.52)	7.28(7.40)	2.94(2.96)	5.58(5.64)
$V_2(\phi) = \frac{\alpha_2}{e^{K\phi^2}}$	$M_{max} (M_\odot)$	$R (km)$	$R_{Sch} (km)$	$\sigma(10^{-1})$	$z(10^{-1})$
$\alpha_2 = -0.01$	2.42(2.42)	11.89(11.89)	7.13(7.13)	3.00(3.00)	5.81(5.81)
$\alpha_2 = -0.05$	2.43(2.44)	11.88(11.87)	7.16(7.19)	3.01(3.03)	5.87(5.93)
$\alpha_2 = -0.10$	2.44(2.45)	11.95(11.95)	7.19(7.22)	3.01(3.02)	5.85(5.90)
$V_3(\phi) = \frac{\alpha_3\phi^2}{1+e^{K\phi^2}}$	$M_{max} (M_\odot)$	$R (km)$	$R_{Sch} (km)$	$\sigma(10^{-1})$	$z(10^{-1})$
$\alpha_3 = -0.01$	2.43(2.44)	11.89(11.89)	7.16(7.19)	3.01(3.03)	5.86(5.91)
$\alpha_3 = -0.05$	2.45(2.47)	11.97(11.97)	7.22(7.28)	3.02(3.04)	5.88(5.98)
$\alpha_3 = -0.10$	2.48(2.52)	11.94(12.05)	7.31(7.43)	3.06(3.08)	6.06(6.15)

of gravitation, consistent with astrophysical observations, is ongoing with great motivation.

TABLE VIII: Structure properties of neutron star in mimetic gravity for FSU2H EoS with $\phi(0) = 1$ ($\phi(0) = 0.8$) and $K = 0.5$.

$V_1(\phi) = \frac{\alpha_1}{\phi^2}$	$M_{max} (M_\odot)$	$R (km)$	$R_{Sch} (km)$	$\sigma(10^{-1})$	$z(10^{-1})$
$\alpha_1 = -0.01$	2.40(2.39)	12.57(12.58)	7.08(7.05)	2.81(2.80)	5.13(5.08)
$\alpha_1 = -0.05$	2.42(2.43)	12.81(12.87)	7.13(7.16)	2.78(2.79)	5.02(5.02)
$\alpha_1 = -0.10$	2.45(2.49)	13.15(13.30)	7.22(7.34)	2.75(2.76)	4.90(4.94)
$V_2(\phi) = \frac{\alpha_1}{e^{K\phi^2}}$	$M_{max} (M_\odot)$	$R (km)$	$R_{Sch} (km)$	$\sigma(10^{-1})$	$z(10^{-1})$
$\alpha_2 = -0.01$	2.39(2.39)	12.53(12.52)	7.05(7.05)	2.81(2.81)	5.12(5.12)
$\alpha_2 = -0.05$	2.40(2.40)	12.51(12.55)	7.08(7.08)	2.83(2.82)	5.17(5.14)
$\alpha_2 = -0.10$	2.41(2.43)	12.59(12.57)	7.11(7.16)	2.82(2.85)	5.15(5.25)
$V_3(\phi) = \frac{\alpha_3\phi^2}{1+e^{K\phi^2}}$	$M_{max} (M_\odot)$	$R (km)$	$R_{Sch} (km)$	$\sigma(10^{-1})$	$z(10^{-1})$
$\alpha_3 = -0.01$	2.40(2.41)	12.56(12.56)	7.08(7.11)	2.82(2.83)	5.13(5.17)
$\alpha_3 = -0.05$	2.42(2.43)	12.59(12.59)	7.13(7.16)	2.83(2.85)	5.19(5.23)
$\alpha_3 = -0.10$	2.48(2.51)	12.66(12.71)	7.31(7.40)	2.89(2.91)	5.38(5.47)

This paper is devoted to study the structure of neutron stars through the use of different state equations in mimetic gravity. Various models of EoS are examined in the context of GR and mimetic gravity. Differentiating between the models of EoS indicated by the measurements of the radius and mass of neutron stars in a theory of gravitation. It was shown that considering a few suitable EoSs, the maximum mass and related radius in mimetic gravity can support the mentioned observational data.

In this paper, we examined eight relativistic/non-relativistic EoSs that seem more realistic and have already received more attention in literature. For the non-relativistic category of EoSs, we considered SLy4, BSK21 and WFF1 models. While for the relativistic set of EoSs, we regarded MPA1, HS (DD2) and FSU2H cases. We also used two hadronic EoSs known as $BH\Lambda\Phi$ and SFHoY as other realistic models. According to the obtained results reflected in different figures and tables, we have found that, in general, the results of mimetic gravity are more consistent with observational data than the GR. Besides, we have shown that the results of mimetic gravity are more or less depending on the functional form of potential and its free parameters. Nonetheless, we have found that the results of full relativistic mean-field-based models of EoSs are in better agreement with observational data than non-relativistic models.

For the three non-relativistic models of EoSs, SLy4, WFF1 and BSK21, we have shown that the mentioned state equations can be improved when we generalize the GR to mimetic gravity. Strictly speaking, regardless of GW190814, other observational evidence can be supported by the results of theoretical counterparts in mimetic gravity for SLy4 and WFF1 models. We should note that the same result can be obtained, equivalently, for BSK21 in GR and mimetic gravity. After that, a relativistic model of EoS can be regarded to examine the possible support of GW190814 data. We have taken the relativistic EoSs MPA1, DD2 and FSU2H into account in GR and mimetic gravity, and found that although such models could not solve our problem in GR, they could remove the inconsistency between the GW190814 data and the theoretical results of previous models in mimetic gravity. In other words, considering these three EoSs are excellent candidates for investigation of neutron star structures in mimetic gravity.

According to the presented tables, one can find that for numerical analysis, we have considered the effects of mimetic gravity generalization as a small changes with respect to GR. In other words, we have investigated small values of potential since we did not have the allowed region of free parameters. So, it is interesting to find permitted region of free parameters of mimetic gravity (its potential) based on observational cosmology or fundamental conceptions of high energy physics, and study the effects of mimetic gravity when it is far from the GR. Besides, taking the modification of the mass-radius relation in mimetic gravity into account, it will be interesting to study the thermal evolution of neutron stars. In other words, it is attractive to investigate the cooling process of isolated neutron stars to compare mimetic gravity and GR. So, one can study the possibility of the direct Urca mechanism for rapid cooling or modern theory of cooling based on the nucleon superfluidity depending on the chosen EoS. Keeping the results of this paper and the mentioned suggestions in mind, we can analyze the behavior of hybrid neutron stars or quark stars as well as other compact objects in mimetic gravity. All these points are under considerations.

As a final point, Astashenok et al. in Ref. [94] have studied the structure of neutron stars in mimetic gravity. They have obtained some interesting results about the structure of massive neutron stars. But, they had not compared their results with observational data. Nonetheless, observational data such as GW170817, PSR J0740+6620, PSR J2215+5135, NICER data on PSR J0030+0451, and GW190814 give us essential information on massive compact objects e.g., neutron stars. In this work, we extended the work of Astashenok et al. by comparing observational data with mimetic theory of gravity. In other words, to obtain a good agreement between theory and observational data, we evaluated the structure of neutron stars in GR and mimetic gravity.

Acknowledgments

We are grateful to the anonymous referee for the insightful comments. SHH and HN thank Shiraz University Research Council. The work of BEP has been supported by University of Mazandaran under title "Evolution of the Masses of Celestial Compact Objects in Various Gravity".

-
- [1] R. C. Tolman, *Phys. Rev.* 55 (1939) 364.
 - [2] J. R. Oppenheimer, and G. M. Volkoff, *Phys. Rev.* 55 (1939) 374.
 - [3] S. H. Hendi, G. H. Bordbar, B. Eslam Panah, and S. Panahiyan, *JCAP* 09 (2016) 013.
 - [4] D. Momeni, M. Faizal, K. Myrzakulov, and R. Myrzakulov, *Eur. Phys. J. C* 77 (2017) 37.
 - [5] S. H. Hendi, G. H. Bordbar, B. Eslam Panah, and M. Najafi, *Astrophys. Space Sci.* 358 (2015) 30.
 - [6] S. Capozziello, M. De Laurentis, S. D. Odintsov, and A. Stabile, *Phys. Rev. D* 83 (2011) 064004.
 - [7] A. V. Astashenok, S. Capozziello, and S. D. Odintsov, *JCAP* 12 (2013) 040.
 - [8] A. S. Arapoglu, C. Deliduman, and K. Y. Eksi, *JCAP* 07 (2011) 020.
 - [9] K. Zhou, Z. -Y. Yang, D. -C. Zou, and R. -H. Yue, *Chin. Phys. B* 21 (2012) 020401.
 - [10] A. V. Astashenok, S. Capozziello, and S. D. Odintsov, *JCAP* 01 (2015) 001.
 - [11] S. Capozziello, M. De Laurentis, R. Farinelli, and S. D. Odintsov, *Phys. Rev. D* 2 (2016) 023501.
 - [12] A. V. Astashenok, S. D. Odintsov, and A. de la Cruz-Dombriz, *Class. Quant. Grav.* 20 (2017) 205008.
 - [13] A. V. Astashenok, S. Capozziello, S. D. Odintsov, and V. K. Oikonomou, *Phys. Lett. B* 811 (2020) 135910.
 - [14] R. Lobato et al., *JCAP* 12 (2020) 039.
 - [15] G. A. Carvalho et al., *Eur. Phys. J. C* 80 (2020) 483.
 - [16] R. V. Lobato, G. A. Carvalho, and C. A. Bertulani, *Eur. Phys. J. C* 81 (2021) 1013.
 - [17] A. V. Astashenok, S. Capozziello, S. D. Odintsov, and V. K. Oikonomou, *EPL* 136 (2021) 59001.
 - [18] J. M. Z. Pretel, S. E. Jorás, R. R. Reis, and J. D. V. Arbañil, *JCAP* 08 (2021) 055.
 - [19] R. -H. Lin, X. -N. Chen, and X.-H. Zhai, *Eur. Phys. J. C* 82 (2022) 308.
 - [20] S. H. Hendi, G. H. Bordbar, B. Eslam Panaha, and S. Panahiyan, *JCAP* 07 (2017) 004.
 - [21] B. Eslam Panah, G. H. Bordbar, S. H. Hendi, R. Ruffini, Z. Rezaei, and R. Moradi, *Astrophys. J* 848 (2017) 24.
 - [22] A. Saffer, and K. Yagi, *Phys. Rev. D* 104 (2021) 124052.
 - [23] K. V. Staykov, and R. Z. Zheleva, *Eur. Phys. J. C* 82 (2022) 108.
 - [24] R. Xu, Y. Gao, and L. Shao, *Phys. Rev. D* 105 (2022) 024003.
 - [25] I. Prasetyo, H. Maulana, H. S. Ramadhan, and A. Sulaksono, *Phys. Rev. D* 104 (2021) 084029.
 - [26] T. Harada, *Phys. Rev. D* 57 (1998) 4802.
 - [27] E. Barausse, C. Palenzuela, M. Ponce, and L. Lehner, *Phys. Rev. D* 87 (2013) 081506(R).
 - [28] D. D. Doneva, S. S. Yazadjiev, N. Stergioulas, and K. D. Kokkotas, *Phys. Rev. D* 88 (2013) 084060.
 - [29] M. Shibata, K. Taniguchi, H. Okawa, and A. Buonanno, *Phys. Rev. D* 89 (2014) 084005.
 - [30] R. F. P. Mendes, and N. Ortiz, *Phys. Rev. D* 93 (2016) 124035.
 - [31] H. O. Silva, and N. Yunes, *Phys. Rev. D* 99 (2019) 044034.
 - [32] E. Barausse, *Phys. Rev. D* 100 (2019) 084053.
 - [33] K. Kim, J. J. Oh, C. Park, and E. J. Son, *Phys. Rev. D* 103 (2021) 044052.
 - [34] T. Boyadjiev, P. Fiziev, and S. Yazadjiev, *Class. Quantum Grav.* 16 (1999) 2359.
 - [35] T. Wiseman, *Phys. Rev. D* 65 (2002) 124007.
 - [36] J. A. Faber, P. Grandclément, and F. A. Rasio, *Phys. Rev. D* 69 (2004) 124036.
 - [37] C. Deliduman, K. Y. Eksi, and V. Keleş, *JCAP* 05 (2012) 036.
 - [38] H. Sotani, *Phys. Rev. D* 86 (2012) 124036.
 - [39] C. Deliduman, K. Y. Eksi, and V. Keles, *JCAP* 05 (2012) 036.
 - [40] S. Meyer, F. Pace, and M. Bartelmann, *Phys. Rev. D* 86 (2012) 103002.
 - [41] N. Chamel, P. Haensel, J. L. Zdunik, and A. F. Fantina, *Int. J. Mod. Phys. E* 22 (2013) 1330018.
 - [42] M. Orellana, F. García, F. A. T. Pannia, and G. E. Romero, *Gen. Relativ. Gravit* 45 (2013) 771.
 - [43] T. Harko, F. S. N. Lobo, M. K. Mak, and S. V. Sushkov, *Phys. Rev. D* 88 (2013) 044032.
 - [44] M. Orellana, F. Garcia, F. A. Teppa Pannia, and G. E. Romero, *Gen. Rel. Grav.* 45 (2013) 771.
 - [45] J. D. V. Arbanil, J. P. S. Lemos, and V. T. Zanchin, *Phys. Rev. D* 88 (2013) 084023.
 - [46] H. O. Silva, H. Sotani, E. Berti, and M. Horbatsch, *Phys. Rev. D* 90 (2014) 124044.
 - [47] A. V. Astashenok, S. Capozziello, and S. D. Odintsov, *Phys. Rev. D* 89 (2014) 103509.
 - [48] Y. Brihaye, and J. Riedel, *Phys. Rev. D* 89 (2014) 104060.
 - [49] R. Goswami, A. M. Nzioki, S. D. Maharaj, and S. G. Ghosh, *Phys. Rev. D* 90 (2014) 084011.
 - [50] K. Glampedakis, G. Pappas, H. O. Silva, and E. Berti, *Phys. Rev. D* 92 (2015) 024056.
 - [51] A. Das, F. Rahaman, B. K. Guha, and S. Ray, *Astrophys. Space Sci.* 358 (2015) 36.
 - [52] K. V. Staykov, D. D. Doneva, S. S. Yazadjiev, and K. D. Kokkotas, *Phys. Rev. D* 92 (2015) 043009.
 - [53] G. H. Bordbar, S. H. Hendi, and B. Eslam Panah, *Eur. Phys. J. Plus.* 131 (2016) 315.
 - [54] A. Cisterna, T. Delsate, L. Ducobu, and M. Rinaldi, *Phys. Rev. D* 93 (2016) 084046.

- [55] A. Maselli, H. O. Silva, M. Minamitsuji, and E. Berti, *Phys. Rev. D* 93 (2016) 124056.
- [56] M. Pace, and J. L. Said, *Eur. Phys. J. C* 77 (2017) 283.
- [57] T. Gupta, B. Majumder, K. Yagi, and N. Yunes, *Class. Quantum Grav.* 35 (2018) 025009.
- [58] A. Wojnar, *Eur. Phys. J. C* 78 (2018) 421.
- [59] R. Kase, and S. Tsujikawa, *JCAP* 09 (2019) 054.
- [60] J. L. Blázquez-Salcedo, F. S. Khoo, and J. Kunz, *EPL*, 130 (2020) 50002.
- [61] C. Adam, M. Huidobro, R. Vazquez, and A. Wereszczynski, *JCAP* 08 (2020) 041.
- [62] A. H. Chamseddine, and V. Mukhanov, *JHEP* 11 (2013) 135.
- [63] S. D. Odintsov, and V. K. Oikonomou, *Phys. Rev. D* 93 (2016) 023517.
- [64] Y. Zhong, and D. Sáez-Chillón Gómez, *Symmetry*. 10 (2018) 170.
- [65] S. Vagnozzi, *Class. Quantum Grav.* 34 (2017) 185006.
- [66] A. Casalino, M. Rinaldi, L. Sebastiani, and S. Vagnozzi, *Phys. Dark Universe*. 22 (2018) 108.
- [67] A. Casalino, M. Rinaldi, L. Sebastiani, and S. Vagnozzi, *Class. Quantum Grav.* 36 (2018) 017001.
- [68] A. H. Chamseddine, and V. Mukhanov, *JCAP* 17 (2017) 009.
- [69] A. H. Chamseddine, and V. Mukhanov, *Eur. Phys. J. C* 77 (2017) 1.
- [70] P. Haensel, A. Y. Potekhin and D. G. Yakovlev, *Neutron Stars 1: Equation of State and Structure, Astrophysics and Space Science Library, Neutron Stars*. Springer-Verlag, New York, 2007, 10.1007/978-0-387-47301-7.
- [71] B. P. Abbott et al. (The LIGO Scientific Collaboration and the Virgo Collaboration), *Phys. Rev. Lett.* 121 (2018) 161101.
- [72] F. Douchin, and P. Haensel, *Astron & Astrophys.* 380 (2001) 151.
- [73] R. B. Wiringa, V. Fiks, and A. Fabrocini, *Phys. Rev. C* 38 (1988) 1010.
- [74] A. F. Fantina, N. Chamel, J. M. Pearson, and S. Goriely, *J. Phys: Conference Series*. 342 (2012) 012003.
- [75] H. Mütter, M. Prakash, and T. L. Ainsworth, *Phys. Lett. B* 199 (1987) 469.
- [76] M. Hempel, and J. Schaffner-Bielich, *Nucl. Phys. A* 837 (2010) 210.
- [77] Fischer, T., M. Hempel, I. Sagert, Y. Suwa, and J. Schaffner-Bielich, *Eur. Phys. J. A* 50 (2014) 46.
- [78] L. Tolos, M. Centelles, and A. Ramos, *Publ. Astron. Soc. Austral.* 34 (2017) e065, [arXiv:1708.08681].
- [79] R. Negreiros, L. Tolos, M. Centelles, A. Ramos, and V. Dexheimer, *Astrophys. J.* 863 (2018) 104.
- [80] C. Providencia, M. Fortin, H. Pais, and A. Rabhi, *Astron. Space Sci.* 6 (2019) 13.
- [81] S. Banik, M. Hempel, and D. Bandyopadhyay, *Astrophys. J. Suppl.* 214 (2014) 22.
- [82] M. Fortin, M. Oertel, and C. Providencia, *Publ. Astron. Soc. Austral.* 35 (2018) 44.
- [83] A.W. Steiner, M. Hempel, and T. Fischer, *Astrophys. J.* 774 (2013) 17.
- [84] S. Typel, G. Röpke, T. Klähn, D. Blaschke, and H. H. Wolter, *Phys. Rev. C* 81 (2010) 015803.
- [85] W. -C. Chen, and J. Piekarewicz, *Phys. Rev. C* 90 (2014) 044305.
- [86] J. S. Read, B. D. Lackey, B. J. Owen, and J. L. Friedman, *Phys. Rev. D* 79 (2009) 124032.
- [87] G. Raaijmakers, T. E. Riley, and A. L. Watts, *MNRAS* 478 (2018) 2177.
- [88] B. Kumar, and P. Landry, *Phys. Rev. D* 99 (2019) 123026.
- [89] H. T. Cromartie et al., *Nature Astronomy*. 4 (2020) 72.
- [90] M. Linares, T. Shahbaz, and J. Casares, *Astrophys. J.* 859 (2018) 54.
- [91] M. C. Miller et al., *Astrophys. J. Lett.* 887 (2019) L24.
- [92] T. E. Riley et al., *Astrophys. J. Lett.* 887 (2019) L21.
- [93] B. P. Abbott et al., *Astrophys. J. Lett.* 892 (2020) L3.
- [94] A. V. Astashenok, and S. D. Odintsov, *Phys. Rev. D* 94 (2016) 063008.